A review of the optical properties of alloys and intermetallics for plasmonics

M G Blaber, M D Arnold and M J Ford*
Institute for Nanoscale Technology, Department of Physics and Advanced Materials, University of Technology Sydney, PO Box 123, Broadway, NSW 2007, Australia

*Mike.Ford@uts.edu.au

Abstract. Alternative materials are required to enhance the efficacy of plasmonic devices. We discuss the optical properties of a number of alloys, doped metals, intermetallics, silicides, metallic glasses and high pressure materials. We conclude that due to the probability of low frequency interband transitions, materials with partially occupied d-states perform poorly as plasmonic materials, ruling out many alloys, intermetallics and silicides as viable. The increased probability of electron-electron and electron-phonon scattering rules out many doped and glassy metals.

Contents

1. Introduction

As nanofabrication techniques become increasingly fast and accurate, the performance of plasmonic systems relies less and less on structure fabrication and more on the fundamental limitations of the

underlying materials. Plasmonics has seen an exponential growth, due mainly to the sheer diversity of applications, from optical cloaking [1] to superlensing [melville2005, pendry2000] as well as single molecule surface enhanced raman spectroscopy [2], parasite therapy [3] and optical circuits[4] with high speed optical switching[5, 6].

A number of studies have been performed comparing the plasmonic merit of different metals (see e.g. [7]), and although the alkali metals have increased performance over the noble metals at many frequencies and permittivities, experimental convenience or necessity of inertness dictates that the noble metals are used more frequently.

The free electron character of the alkali and noble metals plays a pivotal role in their plasmonic performance. As the number of free electron metals in the periodic table is severely limited, use of doped metals, alloys and intermetallics to tune the frequency and permittivity response of materials, while simultaneously reducing chemical reactivity and loss, seems an obvious choice.

The concept of loss mitigation by the introduction of gain materials into plasmonic devices is an alternative, though technically more challenging approach. The idea was introduced by Ramakrishna and Pendry [8] who investigated the affect of a gain material replacing the dielectric layers in a multilayer superlensing stack. The imaginary component of the frequency dependent dielectric function $\varepsilon(\omega) = \varepsilon' + i\varepsilon''$, which describes the phase lag of the electrons behind the applied electric field, is negated by a material with a negative effective phase contribution $\varepsilon_{\text{gain}}(\omega) = \varepsilon' - i\varepsilon''$.

The fluorescent dye Rhodamine 6G has been used to compensate for loss in both Local Surface Plasmon (LSP)[9] and propagating Surface Plasmon Polariton (SPP) [9] based systems. Increased confinement of light in metallic waveguides causes a substantial increase in the optical loss. The introduction of gain materials into these systems was proposed by Maier [10]. Quantum dots have been proposed [11] and demonstrated [12] to reduce this loss.

In addition to increased optical loss due to confinement, a number of damping mechanisms contribute to the plasmonic performance of real systems. The effect of grain boundaries in gold films has been discussed quantitatively by Kuttge *et al* where they showed that the characteristic decay length of a propagating SPP mode would be reduced by a grain size dependent factor [13]. Similar effects are apparent in systems with features smaller than the average electron mean free path, and such surface scattering has a significant impact on the optical response of small particles[14] and thin shells (see eg [15]). In addition to surface scattering, the introduction of surfaces allows for the decay of plasmons into electron-hole pairs via surface states (see for example [16] [17]).

It is possible to optimize [18] the size, shape and composition of a multilayer metal system to get the optimum resonance at a particular wavelength, for example to match the absorption profile of a fluorescent dye. Although such systems present yet another way to optimize a plasmonic system, here we shall focus on homogenous systems.

In addition to the conventional methods for tuning the optical response of plasmonic systems, namely modification of structure size and shape; varying the composition of alloyed and intermetallic nanostructures can be used to tune the response. Many studies have investigated the optical properties of noble metal alloy nanoparticles, most notably the Ag-Au alloys, where the plasmon absorption maximum varies linearly from the elemental Ag value of 380nm to the elemental Au value of 520nm as the stoichiometry is varied [19, 20]. This leads one to erroneously assume that the response can be modeled using a simple, linear combination of the experimental dielectric functions. However, this is

not the case and a more rigorous description in terms of the movement of the optical gap and Fermi energy is required. Other alloys are also in use in plasmonics, for example Chiu *et al* [21]describe a synthesis technique for producing NiAu alloy nanoparticles in various stoichiometries with the additional property of magnetism. The absorption efficiency of the particles, and hence the plasmon efficacy, reduces with increasing Ni. Other alloys such as the Cu/Zn system show more complex behaviour, with 95% Cu, 5% Zn particles having a higher absorption efficiency than the 100%, 70% and 30% Cu particles[22]. Fabrication of Sn-based intermetallic nanoparticles has resulted[23] in a multitude of shapes including some similar to the familiar split ring resonator often used in meta-materials[24]. Ferrando *et al* have recently published a comprehensive review of nano-alloys and their optical and catalytic properties [25].

Al/Ga and Au/Ga nanocomposites have been used in high speed plasmon polariton modulation [krasavin2006, macdonald2007], and we shall discuss some of the interesting properties of liquid metals in section 7.1.

Although we shall focus mainly on bulk materials, there are particular alloy combinations which do not have stable bulk phases but do however alloy when structured on the nanoscale (see for example FeAg [26]).

To date, reasonably few intermetallic compounds have been used in plasmonics with the main candidates being $AuAl_2$ [27] and MgB_2 [kussow2007, limberopoulos2009], with other examples including the Heussler type compound Co_2FeGa [28] and Au_3Zn [29]. Nanoparticles made of the latter show slightly increased absorption efficiency over comparable gold particles.

The transition metal silicides are particularly interesting in light of the ease at which waveguides can be constructed in silicon using conventional semiconductor manufacturing techniques. The transition metals can be masked onto the surface and diffused into silicon, creating guiding structures. In section 5 we discuss their optical properties.

West *et al* have recently discussed the merits of a number of alternative plasmonic systems [30] which we shall not discuss here - namely graphene, semiconductors and phonon polariton materials such as SiC. Here, we present a complimentary review focusing on the electronic properties of some materials not discussed in detail by West *et al*. We largely discount the technical challenges that the utilisation of these materials may impose on device fabrication.

This paper is structured as follows: in Section 2 we shall discuss the necessary electronic features of a good plasmonic material and the properties of some metals. In Sections 3-7 we will discuss the optical properties of other plasmonic materials, which encompass five classes of materials as follows. (3) Alloys - includes mainly non-stoichiometric materials, doped materials and nanograined materials. (4) Intermetallic compounds. (5) Silicides. (6) Systems under pressure. (7) Metallic glasses, liquids and amorphous alloys.

2. Plasmonic materials: Definitions and review of metals

2.1 Quality factors and the ideal plasmonic material

The complex dielectric function $\varepsilon(\omega) = \varepsilon' + i\varepsilon''$ fully describes the macroscopic electronic response of a material. It is possible to excite a surface plasmon resonance at any frequency for which the real part of the permittivity is less than zero. The quality of the associated resonance depends on the value of the

imaginary permittivity at this frequency. For the ideal free electron gas, the dielectric function is usually written in the form of a Drude model:

$$\varepsilon_D(\omega) = 1 - \frac{\omega_p^2}{\omega(\omega + i/\tau)} \tag{1}$$

The plasma frequency, ω_p is a function of the electron mass and density, and the phenomenological scattering time τ is sometimes replaced with a scattering frequency γ that encompasses all scattering mechanisms including electron-electron, electron-phonon, surface and defect interactions. The bare plasma frequency can be determined by calculating the transition rate at the Fermi surface in the limit of zero energy and momentum transfer [31].

$$\omega_p^2 = \frac{8\pi}{3V} \sum_{i,\mathbf{k}} |\mathbf{P}_{i,i,\mathbf{k}}|^2 \delta(E_{i,\mathbf{k}} - E_{\mathrm{F}}), \tag{2}$$

where P is the momentum matrix element with wavevector $\mathbf{k}$ within band i. This can also be written:

$$\omega_p^2 = \frac{8\pi}{3V} \sum_{i,\mathbf{k}} \left| \frac{dE_{i,\mathbf{k}}}{d\mathbf{k}} \right|^2 \delta(E_{i,\mathbf{k}} - E_{\mathrm{F}}) \tag{3}$$

where $E_{i,k}$ is just the energy of the ith band at wavevector $\mathbf{k}$. Thus the bare plasma frequency is just a sum of the gradient of bands at the Fermi surface. In section 6 we will comment on the effect of pressure on the gradient of the bands at the Fermi energy, and in section 3 we shall discuss doping as a method of modifying the Fermi energy.

In real materials, the plasma frequency is shifted from the bare plasma frequency (Eqn 2,3) due to screening by interband transitions, which are single particle excitations from the valence to conduction bands. For example, the screened plasma frequency ω_s in silver is at 3.8 eV compared to the bare plasma frequency value of 9.6 eV.

We have reviewed and developed a series of metrics to determine the proficiency of metals to perform in particular plasmonics applications[7]. Although every specific geometry will have a different quality factor, in the limit of low loss and the applicability of electrostatics, two generic limiting cases can be derived, (i) for localized surface plasmon (LSP) applications which include the absorption efficiency of nanospheres and nanoshells, and the resolving power of a multilayer and the 'poor mans' superlens and (ii) for extended modes such as surface plasmon polaritons (SPP) and extended LSP modes of ellipsoids.

$$Q_{\mathrm{LSP}} = -\varepsilon'/\varepsilon'', \qquad\qquad Q_{\mathrm{SPP}} = \varepsilon'^2/\varepsilon''. \tag{4a,b}$$

In the quasistatic regime, where the features of the plasmonic system are much smaller than the wavelength of light, localized surface plasmons depend on the dielectric function linearly, whereas SPPs depend on the square of the real part. In the limit of low loss, the quality factors can be written in terms of the complex refractive index $m = n + ik$:

$$Q_{\mathrm{LSP}} = k/2n, \qquad\qquad Q_{\mathrm{SPP}} = k^3/2n, \tag{5a,b}$$

or the frequency dependent complex optical conductivity $\sigma(\omega) = \sigma_1(\omega) + i\sigma_2(\omega)$:

$$Q_{\text{LSP}} = \frac{\sigma_2 - \omega/4\pi}{\sigma_1}, \qquad Q_{\text{SPP}} = \frac{(\omega - 4\pi\sigma_2)^2}{4\pi\sigma_1\omega}. \qquad (6\text{a,b})$$

By substituting the Drude model (1) into the quality factors (4) and solving for maximum quality we arrive at: [32]

$$Q_{\text{LSP}}^{\max} = \frac{2(\omega_p^2 - \gamma^2)^{3/2}}{3\gamma\omega_p^2\sqrt{3}}, \qquad Q_{\text{SPP}}^{\max} = \frac{\omega_p^2}{2\gamma^2}. \qquad (7)$$

It is now apparent that the most important factor is a large bare plasma frequency to damping ratio ω_p/γ. In the event that the scattering rate is unknown, it is often sufficient to make the approximation:

$$\gamma(T) = \varepsilon_0 \omega_p^2 \rho_{\text{DC}}(T), \qquad (8)$$

where $\rho_{\text{DC}}(T)$ is the temperature dependent DC resistivity and ε_0 is the permittivity of free space.

2.2 A review of the optical properties of metals

In contrast to gold, the band edge (that is, the frequency at which interband transitions become allowed) in silver is at a frequency above the screened plasma frequency, so that surface modes cannot decay into electron hole-pairs. In gold, the situation is more problematic, since for permittivities $-\varepsilon' < 2$ the surface plasmons decay into electron hole pairs, resulting in a much reduced quality factor at these frequencies.

Unfortunately, the effect of interband transitions is much less localized in frequency than this simple picture portrays. Consider a simple Gaussian distribution representing transitions from some valence to conduction band. The transitions are centered at some frequency μ with distribution σ which approximately describes the dispersion of the bands in the metal, and a number α which describes the number of electrons involved in the transitions (and simultaneously the variation in angular momentum character across the Brillouin zone). The interband spectrum now looks like:

$$\varepsilon_{\text{ib}}''(\omega) = \frac{\alpha}{\sqrt{2\pi\sigma^2}} \exp\left(-\frac{(\omega - \mu)^2}{2\sigma^2}\right) \qquad (9)$$

We now use a Kramers-Kronig integration to determine the real part of the spectrum,

$$\varepsilon_{\text{ib}}'(\omega) = 1 + \frac{2}{\pi} P \int_0^\infty \frac{\Omega \varepsilon_{\text{ib}}''(\Omega)}{\Omega^2 - \omega^2} d\Omega \qquad (10)$$

where P indicates the principal part of the integral, and we set $\omega = 0$:

$$\varepsilon_{\text{ib}}'(0) = 1 + \frac{2}{\pi} \int_0^\infty \frac{\varepsilon_{\text{ib}}''(\Omega)}{\Omega} d\Omega \qquad (11)$$

which can be approximated by $\varepsilon_{\text{ib}}'(0) \approx 1 + 2\alpha/\pi\mu$ if $\mu \gg \sigma$. This of course has the effect that even at frequencies well below the band edge, the real part of the permittivity has additional positive component which degrades the local surface plasmon quality factor:

$$Q_{\text{LSP}}^{\max} = \frac{2(\omega_p^2 - 2\gamma^2[1 + \alpha/\pi\mu])^{3/2}}{3\gamma\omega_p^2\sqrt{6(1 + \alpha/\pi\mu)}} \qquad (12)$$

This is our second criteria for a high quality plasmonic material: *the number of electrons involved in interband transitions must be low, and at the highest possible frequency.* This simple and quite obvious criteria significantly reduces the number of materials that are likely to have favorable optical properties, by the simple fact that all materials with partially occupied d or f states are going to perform poorly across the visible due to interband transitions, and even if the transitions do not extend into the IR, poorly at low frequencies because of the aforementioned residual low frequency effect on the polarizability.

The effect of interband transitions on the maximum value of Q_{SPP} is slightly obscure. For low $\varepsilon'_{ib}(0)$, the frequency for maximum Q_{SPP} is just γ. As $\varepsilon'_{ib}(0)$ increases, maximum Q_{SPP} shifts to lower frequencies. It is apparent from the damping frequencies listed in table 1 that it is not particularly useful to describe the maximum in Q_{SPP}. In fact, when the plasma frequency to damping ratio is large, interband transitions have almost no effect on the magnitude of Q_{SPP}.

In figure 1, we present the maximum values for Q_{LSP} (bold) and the frequencies at which they occur for all non-group-f metals. Due to a combination of high plasma frequency to damping ratios, low probability interband transitions and hence low $\varepsilon'_{ib}(0)$, free electron like metals dominate the periodic table in terms of plasmonic performance. For gold and silver, their quality as plasmonic materials is evident from the sheer number of publications in this area. Reported experimental maximum Q_{LSP} values for silver range from tens [33] to hundreds [34] with the latter matching experimental plasmonic device data more closely [35]. Experimental optical constants for gold show similar variability, with Q_{LSP} values varying between 14 and 34. A number of studies have used the experimental permittivity to compare the plasmonic performance of alkali metals in a number of geometries [7, 36-38]. The Group 13 metals, Ga and In have recently been studied by McMahon *et al* [39] where they report Q_{LSP} values of almost 100 for indium at 3.5 eV using the optical constants of [40], Ga performs better than Sn, Pb, Bi, and Tl over the range 3.5 eV to 12 eV, but still has Q_{LSP} below 10 in this region [39].

The actinides[41] thorium, protactinium[42] and uranium[43] all have interband transitions from f to d states [41], as do Gd and Dy [44]. These metals perform poorly over most frequencies. For a review of the optical properties of the Lanthanides, see [45].

Element — box shows: Frequency of Max QLSP (middle), Maximum QLSP (bottom).
Notes: * wmax is at the limit of the available data; # low requency data not included.

Max Qlsp Key
Colour range
0.00-2.99
3.00-3.99
4.00-6.99
7.00-9.99
10+

Periodic table data (Symbol / Frequency of Max QLSP / Maximum QLSP):

Li	Be													B	C
0.14*	0.20														
28.82	**3.58**													**13.58**	

Na	Mg													Al	Si
1.44	4.00													11.00	
35.09	**9.94**													**13.58**	

K	Ca	Sc	Ti	V	Cr	Mn	Fe	Co	Ni	Cu	Zn	Ga	Ge	As	Se
1.05	0.65*	0.3*	0.20	0.36	0.30	0.07*	0.10*	0.10*	0.15	1.75	3.60#	8.30			
40.68	**3.63**	**1.02**	**2.58**	**4.27**	**2.16**	**1.16**	**2.48**	**2.69**	**2.71**	**10.09**	**3.59**	**3.41**			

Rb	Sr	Y	Zr	Nb	Mo	Tc	Ru	Rh	Pd	Ag	Cd	In	Sn	Sb	Te
0.81	0.36*	1.48*	3.00	0.55	0.38		0.10*	0.30	0.10*	1.14	0.65#	5.10	2.25	3.50	
21.90	**2.85**	**1.41**	**1.16**	**3.39**	**5.38**		**2.03**	**2.10**	**6.52**	**97.43**	**3.63**	**4.60**	**3.50**	**1.33**	

Cs	Ba	Lan	Hf	Ta	W	Re	Os	Ir	Pt	Au	Hg	Tl	Pb	Bi	Po
0.51*	1.91		0.52*	0.58	0.30	0.10*	0.10*	0.40	0.35	1.40	4.20	3.20	5.95	3.50	
11.20	**0.91**		**0.79**	**5.25**	**4.96**	**4.99**	**6.12**	**2.55**	**1.96**	**33.99**	**2.20**	**2.71**	**3.07**	**1.15**	

Figure 1. Periodic table of the elements coloured by maximum Q_{LSP}. Frequencies are in eV. References are provided in appendix A.

Table 1. Optical Constants of metals, including the residual low frequency term caused by interband transitions.

Element	ω_p (eV)	γ (eV)	$\varepsilon'_{ib}(0)$
Ag	9.60	0.0228	3.5
Au	8.55	0.0184	9.6
Al	15.3	0.5984	10.4
Na	5.71	0.0276	1.09
K	3.72	0.0184	1.12

In summary we can characterize the plasmonic performance of materials by considering appropriate ratios of the real to imaginary parts of the permittivity. While the plasma frequency and relaxation time of the Drude model are helpful in this regard, it is also important to consider the shift of permittivity as indicated by the interband component at zero frequency. Considering the best elemental metals, alkalis are free-electron-like but impractical, Au and Ag have significant interband transitions, and Al operates best at very high frequency. These options are restrictive and hence we now consider alternatives to allow more choice of operating frequencies and potentially lower losses.

3 Alloys

Nanograined materials can be effectively modeled using a linear combination of the dielectric functions of the constituent metals, weighted by their respective stoichiometries, with an additional damping term to simulate scattering by grain boundaries [46, 47] [48].

3.1 Noble Metal Alloys

Due to their interesting electronic structure and colour, the optical properties of noble-noble alloys are among the most studied of metallic compounds. Randomly oriented AuCu, AuAg and AgCu alloys were studied by Rivory [49] both experimentally by evaporation onto glass substrates and using the coherent-potential approximation (CPA) (see [50]). The interband transitions in Au-Ag alloys with silver concentrations of (in atomic %): 0, 21, 41, 62, 94 and 100 were measured using transmittance/reflectance and Kramers-Kronig analysis. The spectra of Au-Cu alloys were made with Cu concentrations of 0, 12, 25, 40, 70, 81 and 100 at. %. Ag-Cu alloys were made with Cu concentrations of 0, 6, 8, 30, 43, 55, 94 and 100 at.% but had to be deposited at 150K to prevent ordering. The crystal size for Au-Ag and Au-Cu are in the range of 300nm to 500nm, whereas for Ag-Cu they are roughly 1.5nm. It is evident from the interband transitions in the Ag-Cu spectra that 1.5 nm grains are large enough to exhibit the effects of short range order, which causes bulk like interband transitions to become evident. A reduction in short range order often indicates a reduction in the strength of interband transitions. This effect is particularly noticeable when studying liquid metals (See for example [51-53] and section 7). Highly ordered Ag-Cu alloys exhibit a similar 2.5 eV ε'' peak magnitude and shift [54]. The interband transition spectra of the three random alloys exhibits a simple 'mixing' where all of the alloy transitions can be attributed to those of elemental gold, silver or copper [49]. Rivory *et al* report the onset of interband transitions in Au-Ag shifts continuously from 2.5 eV in pure gold to 3.9 eV for pure silver, the extremes being in excellent agreement with the data of Kreibig [55]. A comparison with the optical data of Johnson and Christy[34] and Weaver *et al*[56] show excellent agreement with the elemental data of Rivory *et al*. For Au-Cu the onset of interband transitions shifts from 2.5 eV for pure gold down to an apparent minima at 2.2 eV for 50 at.% Au where it stays for Au concentrations down to pure copper. Part of this shift is due to a decrease in the lattice

constant [57]. In all three alloys, the metal with larger interband transitions dominates the spectra. The order of transition strength for these three metals is Cu > Au > Ag.

Doping of Cu with Al has been shown to introduce indirect transitions near the L point, and the secondary band edge shifts to lower energies, while the primary band edge generally gets larger with increasing dopant concentration [58]. This effect also occurs for Cu doped with Ga, Zn, Sn, Si and Ge [59].

The random binary alloy Cu-Fe was made by Korn *et al* in various iron concentrations from 0 at.% to 20 at.% [60]. The elemental copper peak at approximately 5 eV does not shift a great deal, indicating that the Fermi level does not shift very much upon alloying, but the transition strength decreases, indicating a reduction in order. This effect occurs in Cu-Mn and to an extent in Cu-Pd and Ag-Pd as well [61]. However, in none of these alloys is the minimum in ε'' less than that of the constituent elements.

Alloying of Ag with Mg and Cd causes an additional peak to appear below the 3.9 eV band edge of elemental silver [62, 63], which itself is reduced and allows for the excitation of bulk plasmons above 5 eV, albeit with reduced efficacy due to the overlap with interband transitions, similar to gold. The addition of Sn causes a dramatic increase in the scattering rate up to 0.6 eV (similar to bulk aluminum), and no additional interband transitions are visible, the band edge seems to maintain the same magnitude and energy as that of elemental silver. The relaxation time increases marginally for the Mg and Cd alloys, with maximum values of approximately 0.2 eV and 0.15 eV respectively. They report $\gamma = 0.04\,\text{eV}$ for elemental silver.

Silver-indium alloys show the interesting property that the transitions that make up the 3.9 eV peak can be shifted upon alloying with indium [64]. The 3.87 eV $L_3 \rightarrow L_2$ transition shifts to higher energies and the 4.03 eV $L_2 \rightarrow L_1$ shifts to lower energies. The magnitude of the 3.9 eV peak decreases with increasing In concentration, but the plasma frequency decreases and the damping frequency increases. The overall effect of alloying on ε'' is to increase the imaginary permittivity, resulting in a minimum of 1.5 at 3.5 eV for 12 at.% indium compared to the minimum value for silver, where $\varepsilon'' = 0.37$. The introduction of Ni defects in gold has a similar effect, increasing the damping frequency due to impurity scattering, but reduces the magnitude of the band edge [65].

3.2 Transition Metal alloys

Thomas and Thurm performed optical experiments on binary alloys of W, Ta, Re and Ir in various stoichiometries [66]. Although the optical properties of the alloys are not linearly dependent on the optical properties of the elements, the magnitude of the interband transition maximum in ε'' always lies in between the maximum values for the elements. The maximum in the interband spectrum shifts as follows through the alloy series: W: 20 at 1.8 eV, Re: 16 at 2.5 eV, Ta: 14 at 3 eV.

The prospects for alloys in general can be summarized by observing that although they allow tuning of the real part of the permittivity, they typically have interband strengths similar to their constituents. Grain size effects in some alloys (e.g. AgCu) may modulate interband transitions at the expense of degraded relaxation time due to scattering in a similar fashion to amorphous materials.

4. Intermetallics

In this section we shall discuss the optical properties of the intermetallic compounds in order of the number of constituent elements. As compounds they allow tuning, but avoid grain issues and can have

totally different properties compared to the reactants. We survey alkali-metal, noble-noble, group 13 binaries, other binaries and some ternary compounds.

4.1 Alkali Metal Binary Intermetallics

Optical measurements of LiAl in the NaTl structure suggest that this compound is an excellent free electron metal with only a small interband transition around 0.55 eV, [67] whereas resistivity measurements present conflicting data, with values around 10 $\mu\Omega$cm [68, 69] compared to silver and gold with values of 1.77 $\mu\Omega$cm and 2.66 $\mu\Omega$cm respectively [70].

We showed recently [71] that some of the alkali noble intermetallics had optical gap to plasma frequency ratios greater than 1, indicating that it was very unlikely that interband transitions would disrupt the optical response of these materials. Unfortunately, calculations of the DC resistivity indicated that the Drude phenomenological scattering rate was too high for these compounds to compete with silver and gold [32]. A comparison of the local surface plasmon quality factors for these materials, alongside experimental data for silver and gold is presented in figure 2.
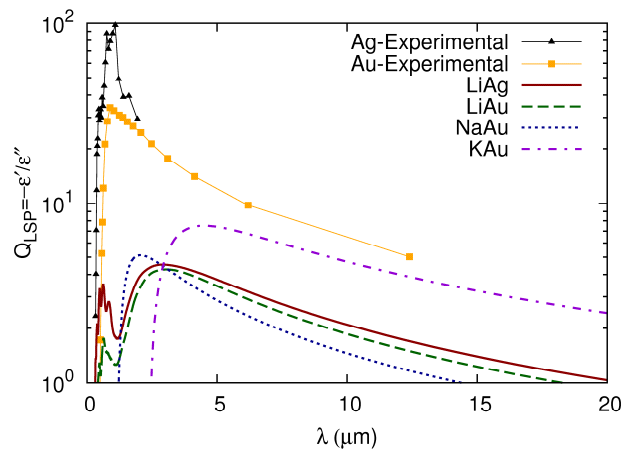

Figure 2. Comparison of calculated local surface plasmon quality factors for the alkali-noble binary intermetallics with the most favourable experimental values for silver [72] and gold [73].

4.2 Noble Binary Intermetallics

Rivory *et al* also investigated the effect of short range ordering on the stoichiometric alloy $AuCu_3$. With increasing order a new peak appears at approximately 3.6 eV. Slightly different results were reported by Scott *et al*; electropolishing of samples post annealing was shown to cause the peak to appear at 3.28 eV [74] but Skriver and Lengkeek noted that electropolishing preferentially etched grains in their polycrystalline sample and reported the peak at 3.6 eV [75]. They also remove the intraband contribution from their experimental data using a Drude fit and note two additional peaks: one at 0.8 eV and another at 1.2 eV. $CoPt_3$ and $MnPt_3$ crystallise in the same structure as $AuCu_3$ but partially occupied *d*-states result in many low energy transition mechanisms, resulting in $Q_{LSP} < 1$ between 1.5 eV and 5.0 eV [76].

The noble - group III alloys crystallize in the CaF_2 structure. The noble atoms occupy sites on an FCC cell and the group III atoms form a simple cubic structure in the centre of the FCC cell [77]. The

discovery of the purple coloured, gold aluminium alloy $AuAl_2$ is often attributed to Sir Roberts-Austen [78]. It has since received a great deal of attention, not only due to its colour and applications in jewellery, but also for its possible applications as an energy efficient window coating. Cortie *et al* [27] measure and calculate the reflectance spectra of $AuAl_2$ using density functional theory. They show an experimentally determined reflectance minima at 2.5 eV, which has been shown to persist for Al:Au ratios of between 3.2:1 to 1:1 [79]. Minor discrepancies appear between the position of the measured and calculated reflectance minima due to self interaction errors. They also measure the reflectance of $PtAl_2$ films which show a reflectance maximum at around 1.9 eV of 55% which steadily decreases into the infrared.

Vishnubhatla *et al* [80] studied the optical properties of $AuAl_2$, $AuGa_2$ and $AuIn_2$. They note that interband transitions appear at 2.2 eV in $AuAl_2$ and are responsible for the reflectance minimum at 2.5 eV. Hsu *et al* note that this transition is not due to Au 5d bands [77]. The onset of interband transitions decreases as the atomic number of the alloying compound increases. $AuGa_2$ has much broader experimental interband transitions in the region around 2 eV than $AuAl_2$ [80, 81]. Calculations show that this broadening is caused by an additional transition at approximately 1.6 eV. When substituting platinum for gold the reflectance minima at 2 eV shifts to 3eV and the reflectance peak at 3 eV shifts to 4 eV. This occurs due to a combination of shift in the 2 eV transition peak to 3.6eV in PtGa2, and an associated shift in the real part of the permittivity. The variation in the position of the transition peak between gold and platinum can be explained by a decrease in energy of the 5d bands of Au in $AuGa_2$ causing the Γ_7 band to be below the Fermi energy [81]. This effect is not seen in $AuAl_2$ or $AuIn_2$ [hsu1994, switendick1969].

Silver indium alloys show the interesting property that the transitions that make up the 3.9 eV peak in silver can be shifted upon alloying with indium [64]. The result is that the 3.87 eV $L_3 \rightarrow L'_2$ transition shifts to higher energies and the 4.03 eV $L'_2 \rightarrow L_1$ shifts to lower energies. Unfortunately, the overall effect is to increase the imaginary permittivity, resulting in a reported minimum of 1.5 at 3.5 eV for 12 at.% indium. The minimum ε'' for silver occurs at approximately 3.5 eV with a value of 0.22. The addition of aluminium into silver also causes a continuous shift in the minimum of ε'' from 0.22 to a value of 1.78 at 2.7 eV [82]. This increase in the minimum of ε'' causes a decrease in the magnitude of the real part of the permittivity, causing the main silver transition at 4 eV to shift to higher energies and its value to shift from 1.75 to just above zero, causing the permittivity of the alloy to become negative for all energies below 7.6 eV [82].

Plasma frequencies for the three CsCl structured Noble alloys AuZn, CuZn and PdIn are shifted quite substantially from their unscreened locations at 11.5 eV, 12.6 eV and 11.0 eV respectively by interband transitions [83]. The biggest shift occurs for PdIn, where the screened plasma frequency is shifted to 2.4 eV. In AuZn the screened plasma frequency ω_s is shifted the least with ε' crossing 0 at 7 eV. The real permittivity for CuZn exhibits a positive region between 2.5 eV and 3.1 eV, giving it a purplish pink colour similar to that of AuZn which is yellow-pink. The interband transition strength is greatest in CuZn and least in PdIn. The onset of transitions appears to occur at approximately 1eV for PdIn and AuZn, and at about 2 eV for CuZn. All three compounds exhibit a transition gap between 2eV and 3eV in the region where ε' becomes steep due to intraband contributions. As the amount of disorder in CuZn is increased the band edge at 2eV reduces and a low energy transition become apparent [84].

Of all the alloys studied here, CsCl structured binary intermetallics show the most promise, with large optical gaps and in some cases, plasma frequencies comparable to silver and gold.

4.3 Group 13 Binary Intermetallics

NiAl, CoAl and FeAl all have major interband contributions to the imaginary part of the permittivity, with the minimum value of ε'' being 10 for CoAl and FeAl at 2.75 eV and 3.25 eV respectively [85]. Of Ni$_3$Al [86], Ni$_3$Ga and Ni$_3$In, only Ni$_3$In shows reasonable Q_{LSP}, with values above 2 at frequencies below 1 eV [87]. DFT calculations on Ni$_3$Al and CoAl both suffer from the effect of partially occupied *d*-states, and exhibit the property that electron self energy corrections shift the interband transitions to lower energies, and hence Rhee *et al* use a negative lambda fitting regime, which corrects their optical spectra into line with experiment.

The optical properties of CoAl and NiAl alloys were determined by Kim *et al* [88] both experimentally and using the linearized augmented plane wave (LAPW) method. Their calculations show very good agreement with experiment below 2.5eV, and accurately describe the onset of interband transitions which occurs at 1eV for CoAl and 2.5 eV for NiAl. The variation in the onset of interband transitions is attributed to a shift in the Fermi energy with the addition of a *d*-electron in nickel. In CoAl, transitions across a band pair along Γ-M -X and X-R are responsible for the low energy transitions. When nickel is substituted for cobalt, the top band becomes occupied and transitions become impossible. The minimum ε'' they report for NiAl is approximately 11 at the low energy edge of their experimental data (1.2 eV) and approximately 4.5 at the high energy edge of their experimental data (6.0 eV) for CoAl. The FP-LAPW method using GGA (PW92 functional) and self energy corrected LDA (LDA + U) exchange correlation functionals were used by Rhee *et al* [89] to calculate the optical properties of FeAl. It was found that both LDA+U and a positive λ fitting routine were required to improve the agreement with experiment as the effects of correlation are known to induce a paramagnetic ground state in FeAl. The experimental spectra exhibits three main transitions at 0.5 eV with magnitude 102, one at 1.5 eV with magnitude 29 and the last at 4 eV with magnitude 12. Transitions below 3 eV occur around the Γ, X and M special points [90]. The minimum in ε'' occurs at the high energy edge of the experimental data at 5 eV with a value of 9.6. The calculations indicate that the transitions decrease over this region. Other groups [91] report maximum transition magnitudes of 55, almost half that of Rhee *et al*.

In 1985 van der Heide *et al* [86] performed ellipsometric spectroscopy on two Ni$_3$Al alloys. One of the samples was an 8mm polycrystalline sample and the other a 3mm single crystal. The sample size limited the accuracy of the results they obtained at energies greater than approximately 5.5eV and hence their measurements extend only from 0.5eV to 5.5eV. They report no noticeable difference between the optical measurements of the two samples.

The most interesting feature in the spectra is a peak in ε'' from about 2.5eV to about 4.5eV. This peak pushes the real part of the permittivity above 0 resulting in two bulk plasmons, one at 3.4eV and another at 3.9eV. An analysis of the infrared Drude tail showed that in the absence of interband transitions the sample would exhibit a bulk plasmon at approximately 9eV (which is quite close to the bulk plasmon of nickel at 10 eV [73]). Unfortunately due to a high damping frequency, the Drude contribution to ε'' grows rapidly at visible wavelengths. Van der Heide *et al* also calculated that interband transitions appear at the optical conductivity from approximately 1eV in Ni$_3$Al and claim that early onset interband transitions are common in *d*-metals. A comparison of the optical conductivity with the Joint Density of States (JDOS) per energy level showed remarkable similarity in their results. This is particularly surprising as they leave the transition matrix elements constant. This means that the

heights of the peaks that are evident in the JDOS/ω are arbitrary, even when compared across the spectrum.

Further investigations by Rhee *et al* showed an increase in interband transitions with non-stoichiometric concentrations as well as increased transition strength with ferromagnetism and temperature [rhee1997, rhee2003]. Rhee *et al* also note that the transitions at 4 eV originate from bands near M along Σ rather than around Γ as reported by [86]. A reduced transition strength is reported by Hsu *et al* [87], which causes the real part of the permittivity to be positive for energies above 2.4 eV. They attribute this to a superior sample surface.

Hsu and Wang [87] recently calculated the optical properties of the alloys Ni_3Al, Ni_3Ga and Ni_3In using DFT with a FP-LAPW basis. They calculated interband transitions between 0eV and 150eV however no ε' results are presented. In similar fashion to the lattice constants reported for the group-13 gold alloys, the Ni_3Al and Ni_3Ga lattice constants are quite similar at 3.571 and 3.589 and the Ni_3In lattice constant is 3.745 about 5% greater than Ni_3Al. The optical calculations overestimate the magnitude of both the 1.0 eV and 2.0 eV transitions in Ni_3Al, the 1.25 eV transition in Ni_3Ga and all transitions in Ni_3In. Notably, the minimum in the experimental ε'' for Ni_3In occurs at 1.35 eV and has a value of 0.5; at this energy the real part has value of -3.5, giving a Q_{LSP} of 7.

The Laves phase ($MgCu_2$ structure) Lanthanide group 13 intermetallics $LaAl_2$ $CeAl_2$ $PrAl_2$ $YbAl_2$ all have *f*-states very close to the Fermi energy. Interaction with conduction states results in a low energy threshold for interband transitions [lange2000, lee2000]. However, the compounds YAl_2 $LuAl_2$ have their *f*-states centered well above and well below the Fermi energy respectively, resulting in the main interband transition occurring at approximately 2 eV. None of these materials have $Q_{LSP}>1$. The $AuCu_3$ compound $LuAl_3$ also has high lying *f*-states, and the density of states at the Fermi energy of $YbAl_3$ is nearly twice as large compared to $ScLa_3$ and $LuAl_3$ because of partially occupied *f*-states, but interband transitions cause the compound to have no metallic character between 1.5 eV and 5.5 eV [92].

4.4 Other Binary Intermetallics

In $LaSn_3$ the onset of interband transitions occurs at approximately 0.5 eV with the main peak at approximately 1.5 eV [93]. All the transitions between 1 eV and 5 eV can be explained due to the mixing of 4*f* character into states near the Fermi energy, with the dominant transition mechanism arising from La 5*d* to hybrid *f-d-p* states [93]. In $CeSn_3$ the situation is even worse due to increasing 4*f* character of conduction states, which causes partial occupation of *f-d-p* states allowing for additional transition mechanisms. $ThPd_3$ and UPd_3 both exhibit the $TiNi_3$ structure, UPd_3 having partially occupied 5*f*-states and $ThPd_3$ having completely unoccupied 5*f*-states; the onset of interband transitions in both materials is < 1 eV [94]. The interband component of the optical spectra for all these materials is too great to allow for reasonable plasmonic activity.

4.5 Ternary Intermetallics

MgAuSn exhibits the cubic AlLiSi structure (F43m) and is coloured purple due mainly to very strong interband transitions around 3 eV [95]. The transitions are likely due to the parallel band effect which gives aluminium its strong interband component at 1.5 eV. Because the transition in MgAuSn becomes steep at a higher energy, and the material has a lower effective Drude plasma frequency, Kramers-Kronig integration forces the real part of the permittivity into the positive over the region 2.2 eV to 3.1 eV. Interband transitions were calculated using the tight-binding linear muffin orbital (TB-LMTO)

method within the local density approximation. Intraband contributions were included by fitting a Drude damping constant and plasma frequency to experimental data.

The optical properties of the magnetic Heusler alloy Cu_2MnAl have been calculated using a tight binding plane wave [96]. Generally reasonable accord between experiment and theory was apparent below 3.5 eV which included the two main features at 1.5 eV and 2.7 eV. The feature at 1.5 eV also bears similarity to the low energy transition in aluminium, and the 2.7 eV peak is reported to arise from transitions between hybridised conduction bands. Additional studies by Kudryavtsev et al [97] suggest that Q_{LSP} is greater than 1 for frequencies below 1 eV. Damping to plasma frequency ratios of between 8.85 and 10.7 have been measured in samples of Ni_2MnGa depending on the annealing temperature [98] however both Ni_2MnGa and Ni_2MnIn [99] have large low energy interband transitions. Fe_2TiAl has a plasma frequency of 0.22 eV [100], lower than the value of 1.32 eV for Fe_2VGa, which gives a reasonable ω_p / γ value of 29 [101], however interband transitions cover most of the spectrum, disrupting quality.

The most promising of all the alloys studied here is Li_2AgIn alloy. It crystallizes in the NaTl-type structure (Zintl Phase), with 16 atoms per unit cell such that a group of 8 BCC cells make up a cube. The corner atoms of each BCC cell are composed of alternating lithium and indium atoms and the centers of alternating BCC cells are lithium and silver atoms. Zwilling et al [102] report some very interesting results for this compound, the most surprising of which is that at exactly 2 eV the imaginary part of the permittivity is zero. A material such as this would have phenomenal optical properties, most notably, an infinitely sharp resonance. Of course, such a resonance is not really possible, and 'very large' will have to suffice. The real part of the permittivity at 2 eV is also reported by Zwilling et al [102] and a value of -16 is given. Zwilling et al determined the complex permittivity by ellipsometry. Their samples were prepared by melting the constituent metals in various ratios in a furnace at 1000∘ C. The concentration of lithium remained constant while the silver and indium concentrations obeyed the formula $Ag_{2-x}In_x$. At $x = 1$, ε'' in Li_2AgIn is at a minimum of 0.0 at 2.0 eV. In $Li_2Ag_{0.50}In_{1.50}$ the minimum in ε'' increases to above 4, shifts to lower energies and the gradient of the real part becomes less negative. Unfortunately, in the same work, Zwilling et al report the optical properties of Li_2CdIn. According to their data, the imaginary part of the permittivity reaches -2 at approximately -3.1 eV. This violates causality and cannot be correct. It is possible that the cause for this error lies in the extrapolation regime they use in conjunction with the Kramers-Kronig relations, but no reference is made. Overall, this indicates that the proximity of ε'' to zero for Li_2AgIn should be discounted, but not ignored.

We recently [71] calculated the interband component of the imaginary permittivity for a series of materials in the series Alkali$_2$-Noble-Group 13 and Alkali-Noble$_2$-Group 13, with the alkali metals consisting of Li, Na and K, the noble metals Ag and Au and the group 13 metals Al, Ga and In. Figure 3 compares the imaginary permittivity measured by Zwilling et al with calculated interband imaginary permittivity values of our previous work [71] no Drude intraband term is included.
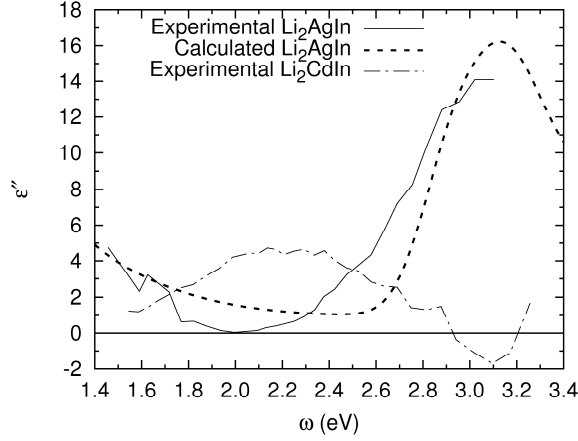
Figure 3. Experimental imaginary permittivity of Zwilling *et al* [102] for Li$_2$AgIn (solid line) and Li$_2$AgCd (dash dot line). Note the non causal region between 2.9 eV and 3.2 eV. Calculated interband imaginary permittivity of Blaber *et al* [71] for Li$_2$AgIn (dashed line) shows the permittivity not going to zero.

In conclusion, the plasmonic quality of intermetallic compounds is heavily reliant on the complexity of the band structure. Interband transitions dominate in materials with large numbers of atoms in the unit cell. If alternative plasmonic materials are going to be realized in the form of intermetallics, binary compounds with only two atoms in the primitive cell that have low lying *d*-states are most likely to be competitive.

5. Silicides

Silicides present an interesting alternative to metals for use in plasmonics. Due to extensive use in metal-oxide-semiconductor field effect transistors (MOSFETs) their optical and electrical characteristics have been widely studied (for a review of their application to MOSFETs see [103]). Moreover, as most of the studied silicides grow epitaxially on silicon, current and future semiconductor manufacturing techniques can be directly applied to the creation of sub-10nm plasmonic devices. In fact device structures amenable to on chip plasmonic information transfer such as nanowires have already been created from silicides [jiang2009, song2007, zhang2006]. Recently, Soref *et al* [104] have proposed the use of Pd$_2$Si as an alternative to gold in SPP based plasmonic devices. They argue that as long as on chip transport requirements are met (i.e. high speed, small size, low loss) then the operating wavelength of the system is irrelevant. To ensure that the mode confinement is reasonable the longest operating wavelength is chosen such that field emanating from the waveguide penetrates no greater than three wavelengths on the air exposed side. Unfortunately, they mistakenly divide all the penetration lengths by a factor of 2π, causing the operating wavelength to be at very low frequencies, where in fact the penetration length reaches hundreds of microns. Nonetheless, their criterion is a good one and we shall use it to assess the plasmonic performance of a number of silicides.

The penetration depth of the tangential component of a surface plasmon polariton traveling along a metallic strip surrounded by air can be approximated by:

$$L_{\text{pen}} = \frac{\lambda}{\text{Re}[\sqrt{-1/(\varepsilon(\omega)+1)}]} \qquad (13)$$

where $\lambda = c/\omega$. Enforcing the condition $L_{\text{pen}}/\lambda = 3$ for a Drude metal reduces to $\varepsilon'(\omega) \approx -10$. The propagation length of such a mode is:

$$L_{\text{prop}} = \frac{1}{2\,\text{Im}[\lambda\sqrt{\varepsilon(\omega)/(\varepsilon(\omega)+1)}]}. \tag{14}$$

Where the frequency is (for a Drude metal):

$$\omega = \sqrt{\frac{\gamma^2(1-\varepsilon') - \omega_p^2}{\varepsilon' - 1}} \tag{15}$$

A summary of the optical properties of some silicides is presented in table 2. We have included the SPP quality factor at the telecommunications wavelength of $1.5\,\mu m$. For comparison, the value for silver is 4522 [30]. We previously noted (see Section 1.2) that a Drude model is sufficient to describe $Q_{\text{SPP}}^{\text{max}}$ as long as the plasma frequency is much larger than the scattering rate - this is of course arises from a significant contribution to the real part of the permittivity that drowns out the effect of interband additions to the imaginary part and any residual effect on the polarizibility that these transitions may incur. However, all the silicides presented in table 2 have small plasma frequency to damping ratios compared to silver and gold. The data for TiSi$_2$ is derived from the plasma frequency and DC resistivity, and although most of the scattering rates calculated from DC resistivity measurements are very close to those extracted from optical data, there is no a priori way of estimating the error. More recent optical constants by Kudryavtsev et al [105] for TiSi$_2$ reduces Q_{SPP} at 1.5 um to 27, down from 1348.

Table 2. Optical constants of various transition metal silicides including surface plasmon polariton quality factors at the telecommunications wavelength λ~1.5μm. Calculated using the collated data of Nava et al [106]. γ_{opt} is the Drude scattering rate extracted from optical constants, and is used - along with the plasma frequency - in the calculation of Q_{SPP}. In the case where γ_{opt} was not available, γ_{ρ} - the scattering rate calculated from the DC resistivity – was used instead. $Q_{\text{SPP}}^{\text{max}}$ corresponds to Q_{SPP} at the damping frequency (see section 2.1).

	ω_p (eV)	γ_{opt} (eV)	γ_{ρ} (eV)	Q_{SPP} (0.8 eV)	$Q_{\text{SPP}}^{\text{max}}$	L_{prop} (μm) when $L_{\text{pen}}/\lambda = 3$
VSi$_2$	2.75	0.070	0.069	112	769	61.64
NbSi$_2$	2.3	0.051	0.052	100	1030	9.59
TaSi$_2$	2.6	0.060	0.055	115	942	64.45
NiSi$_2$	4.6	0.150	0.157	160	471	80.89
NiSi	3.8	0.035	0.035	470	5887	234.80
Ni$_3$Si	3.4	0.044	0.149	293	2999	150.03
V$_5$Si$_3$	2.9	0.143	0.149	60	203	33.82
V$_3$Si	3.4	0.115	0.114	109	431	57.27
HfSi$_2$	1.5	-	0.026	55	1620	48.70
GdSi$_2$	2.4	-	0.091	62	348	36.40
ErSi$_2$	1.3	-	0.014	60	4540	70.55
TiSi$_2$	4.2	-	0.015	1348*	38240	661.11
WSi$_2$	1.78	0.020	0.004	127	4003	90.72
Pd$_2$Si	2.8	0.030	-	276	4376	149.20

Doping of transitions metals exhibits similar qualities to doped metals, namely, the screening of interband transitions. The Fe$_{1-x}$Si$_x$ compound studied by Kim et al [107] (figure 4) shows decreasing metallicity with increasing silicon concentration as the density of conduction electrons decreases, this

causes a decrease in the SPP properties of FeSi. However, increasing silicon concentration also screens interband transitions, and for some frequencies and compositions, the LSP quality is greater than that of pure iron.
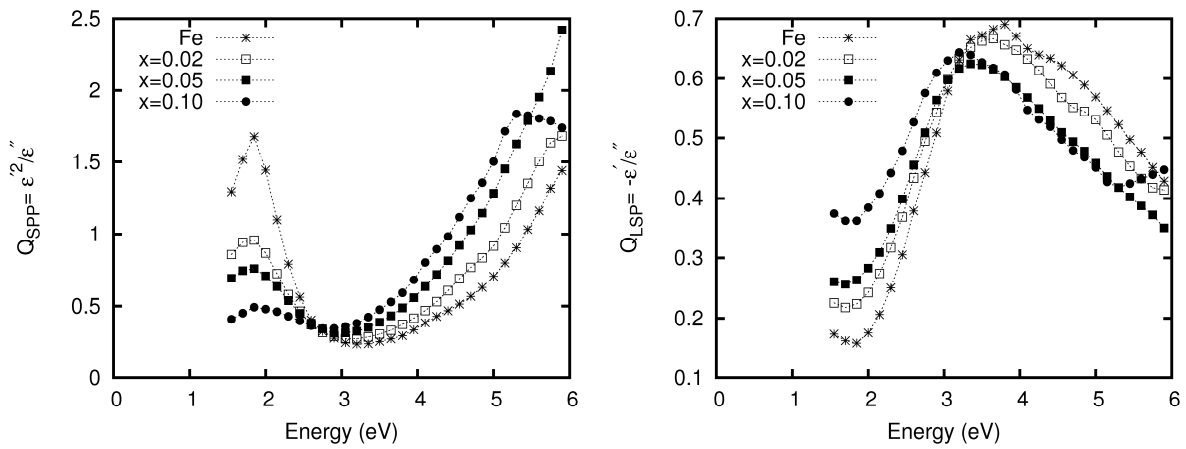

Figure 4. Quality factors for surface plasmons in the structure $Fe_{1-x}Si_x$

In figure 5 we present experimental Q_{SPP} data collated by Nava *et al* [106] and compare it to the Drude model for which optical constants are presented in table 2. Due to the distinct lack of agreement between experimental optical constants and the Drude model for these compounds, or the requirement of frequency-dependent scattering rates, we strongly discourage its use, even at very long wavelengths.

Figure 5. Local surface plasmon quality factors for group 5 transition metal silicides. Black lines: experimental data collated by [106], blue lines: Drude model using parameters from table 2.

The alkali metal silicides have been shown to be semiconductors [108]. The alkaline earth metal silicides exhibit poor metal characteristics (eg CaSi ρ_{DC} =282 μΩcm [109]) semiconductors eg $BaSi_2$ [110] and reasonable metallic character (eg $CaSi_2$ ρ_{DC} =32 μΩcm [109]). Some of the rare earth silicides are metallic, such as GdSi [111] and ErSi [wetzei1991, angot1999] albeit with exceptionally poor plasma frequency to damping ratios ($\omega_p / \gamma \approx 1$) whereas others are semiconductors such as EuSi and YbSi [112].
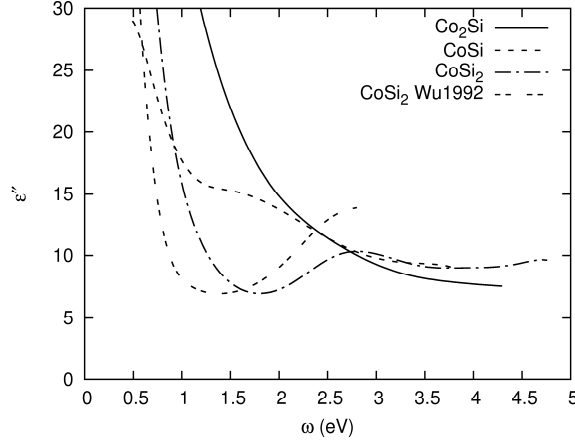
Figure 6. Experimental imaginary permittivity of cobalt silicides in various stoichiometries. Data from Kudryavtsev *et al* [113] and Wu [114].

In summary, although the silicides offer considerable technological conveniences and some of them are potential candidates for guiding long wavelengths (e.g. $TiSi_2$), they are generally poor when compared to other materials and are not suitable for LSP applications.

6. High Pressure Materials

Metals and alloys under pressure has become a very popular topic. Pressure and phase transformations drastically alter the electronic properties of materials, shifting optical gaps, the plasma frequency as well as modifying electron-phonon and electron-electron scattering.

Structural phase transitions, electronic topology transitions and metal-insulator transitions in systems under high pressure open the doors to whole new world of materials for plasmonics. We shall briefly discuss some of these properties, with a focus on pressures sustainable in active devices.

Potentially, an increase in pressure can increase the plasma frequency meeting one of our criteria for a good plasmonic material. However, increasing the band gradient at the Fermi surface, and the possibility of overhauling the topology of the Fermi surface due to pressure induced electron transfer from one band to another can dramatically alter the electron phonon coupling, and hence have a detrimental impact on the phenomenological relaxation time. This change in topology, where previously unoccupied bands cross the Fermi energy is known as an Electronic Topology Transition (ETT). Such transitions can have positive and negative effects. The effects of pressure on the alkali metals has become an exciting topic due to the discovery of novel phase transitions[115], some of which are superconducting (see e.g. [116] and [117]).

The band edge in lithium can be shifted from 3 eV to almost 7 eV by the application of pressures as low as 40 GPa [118]. The magnitude of the band edge is increased from 1.75 in the BCC phase to approximately 2.75 for the FCC and hR1 phases. The FCC phase has a screened plasma frequency to optical gap ratio greater than 1[119].

The introduction of pressure on K causes a more substantial increase in the interband contribution to the permittivity; $\varepsilon_{ib}''(\omega_g)$ increases from less than 1 at 2.2 eV to greater than 7 when the crystal volume is reduced to 45% of the ground state volume [120]. Gao *et al* have studied an anomaly in the resistivity

of SC calcium[121]. They note that the resistance anomaly in SC calcium that occurs at approximately 40 GPa can be attributed to an increase in the electron phonon matrix element and an increase in the plasma frequency due to an ETT from $4s$ to $3d$ states. The pressure dependence of the plasma frequency for some alkali, noble and group 13 elements is shown in figure 7, although we can expect an increase in plasmonic quality with increased plasma frequency, the technical difficulty of operating a plasmonic system under pressure negates any (minor) increases in quality. Additionally, in many cases additional pressure increases resistivity [122].
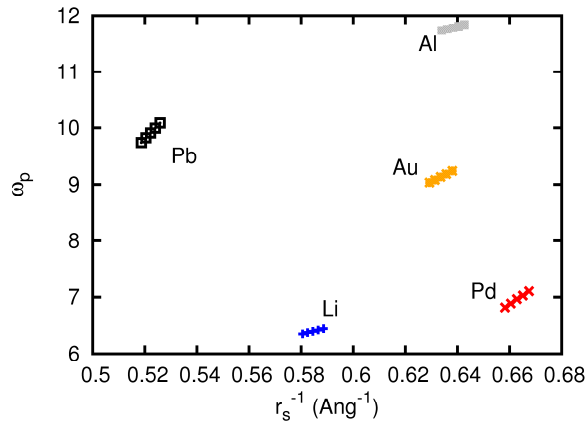

Figure 7. The effect of pressure on the plasma frequency of some metals studied by Sundqvist [123]. r_s is the effective radius for an atom in the unit cell. Pressure increases to the right.

ETTs in the Noble-Group 13 intermetallics AuX_2 under pressure cause additional transition mechanisms at the high symmetry points in the Brillouin zone, presumably reducing the resonance quality [124].

In summary, although topological changes under high-pressure offer the chance to drastically alter material properties, and some of them may exhibit increased plasmon quality (e.g. in Li), others are degraded (K). Further, the pressure required is impractical (although not impossible).

7. Liquid Metals and Glassy/Amorphous Materials

For any purely amorphous system, the concept of k-space is ill-defined, and as such the difference between interband and intraband transitions disappears resulting in a smearing of the band edge. Usually, the smearing occurs down to zero frequency as transitions which are forbidden in the crystalline state become possible with increasing amorphicity. As such, the optical properties of such systems should be well described by the Drude model with a high damping frequency. There are some serious disadvantages to using liquid metals and amorphous alloys in plasmonics, notably, the generally high temperature required to have a metal in a liquid state, and the difficulty in depositing nano-patterned amorphous films. Nonetheless, we shall see that liquid sodium has quite amenable optical properties, and the amorphous silicide PdSi may be useful in plasmonic devices.

7.1 Liquid Metals

The reduced order and increased temperature evident in liquid metals has the effect of shifting the interband transitions to lower energies as they are broadened in a similar fashion to amorphous compounds with the additional drawback of increased electron-electron scattering rate due to increased temperature. Although one would not expect interband transitions in the optical spectra of liquid metals

due to disruption to the periodic potential, even short range order in liquid metals is sufficient to observe interband transitions.

The quality factors Q_{LSP} and Q_{SPP} are presented for liquid and solid Na in figure 8a using the data of Inagaki *et al* [inagaki1976liquid, inagaki1976solid]. Of all the materials in this review, liquid sodium is the first material to exhibit superior plasmonic properties compared to its standard state elemental counterpart. Ingaki *et al* measure the optical constants under a pressure of 2×10^{-9} Torr and at a constant temperature of 120ºC to minimize vaporization. Once the sodium was melted, an oxide coating on the sample was removed in situ by the use of a stainless steel scraper. The Maximum Q_{LSP} of liquid Na is 42.1 [51], whereas for solid Na it is 41.1, and the frequency at which this maximum occurs increases in liquid Na to 2.3 eV from 1.3 eV in the solid. From these parameters for liquid Na we can calculate the scattering rate and plasma frequency for a Drude metal: $\gamma = 0.038$ eV and $\omega_p = 4.16$ eV. There are remnants of the band edge evident in the liquid phase [51], albeit with much reduced magnitude, and a slight shift to higher energies. Helman and Baltensperger [125] argue that this apparent interband component can be explained by frequency dependent scattering due to ion-electron interactions.
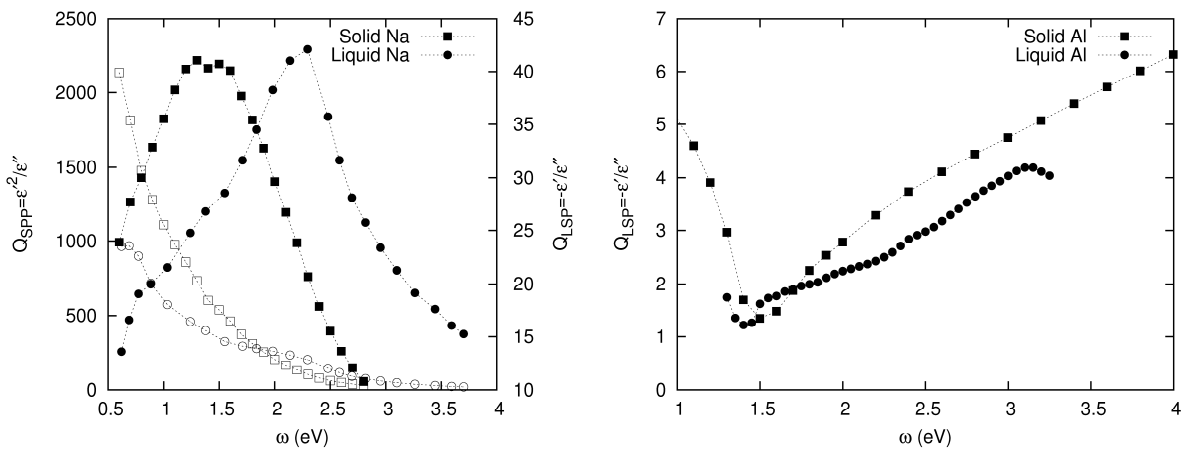

Figure 8. Optical data for A) sodium [inagaki1976liquid, inagaki1976solid] and B) aluminum[126, 127]. Data for solid phase (squares) and liquid phase (circles). Filled symbols represent Q_{LSP} data and open symbols represent Q_{SPP} data.

Q_{LSP} data by Krishnan and Nordine [126] for liquid Al is presented in figure 6b alongside the data for the solid state by Shiles *et al* [127]. The 1.5 eV transition is shifted to lower energies, and there is a noticeable increase in the scattering rate which is not evident in liquid Na. Additionally, the plasma frequency reduces with increasing temperature [128].

Al-Ga and Au-Ga nanocomposites have been employed in high speed modulation of surface plasmon polaritons. The functionality arises from a heating effect in the composite that causes a structural transformation in the gallium [6, 129, 130]. A comparison of local and propagating plasmon modes for liquid and solid gallium is presented in figure 9. Liquid gallium has a significantly superior optical response over the solid phase for a very large wavelength range (100 nm to 20 μm). The maximum Q_{SPP} is 185 at 1.77 μm.

The band edge in liquid silver shifts to higher energies, the onset of interband transitions is not as steep in the liquid phase, and the maximum of the band edge is at 4.5 eV. In copper, the band edge broadens and shifts to lower energies. Both materials have increased scattering rates [131].

The scattering rate in liquid Pb and Sn is an order of magnitude greater than in the solid state [132]. The maximum Q_{LSP} measured for liquid Pb is 1.38 at 3.7 eV, more than 4 times lower than the solid [133].Similarly, Bi has maximum Q_{LSP} of 0.7, 5 times lower than the solid [133].

Mercury and liquid mercury-indium alloys were studied by Hodgson [134]. The scattering rate increases from 1.44 eV to 1.72 eV when the temperature of elemental mercury is increased from 20 C to 200 C. Adding indium to liquid mercury steadily decreases the scattering rate at 20 C and can reach values of 0.8 eV with 33.4 at.% indium.
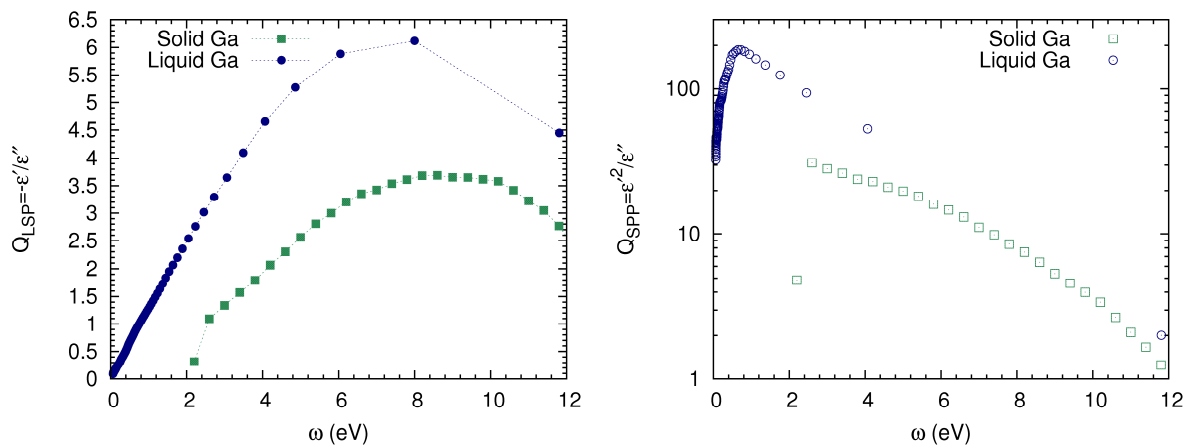

Figure 9. Optical data for solid [135] and liquid [136] gallium A) Q_{LSP} data B) Q_{SPP} data.

Both silicon and germanium exhibit the free electron like Drude tail in the liquid phase at the moderately impractical temperatures of 1600K and 1300K. Fuchs [137] has compared experimental and calculated data for liquid silicon prepared in a variety of ways, and some of the data shows Q_{LSP} can take values greater than 1 at energies above 4 eV.

7.2 Amorphous/Glassy Alloys

Amorphous $Au_{1-x}Si_x$ [138, 139] was the first material discovered to have a damping frequency greater than the optical gap, resulting in exceptionally poor optical properties. The summary of the maximum Q_{LSP} and the frequency at which it occurs is presented in figure 10.
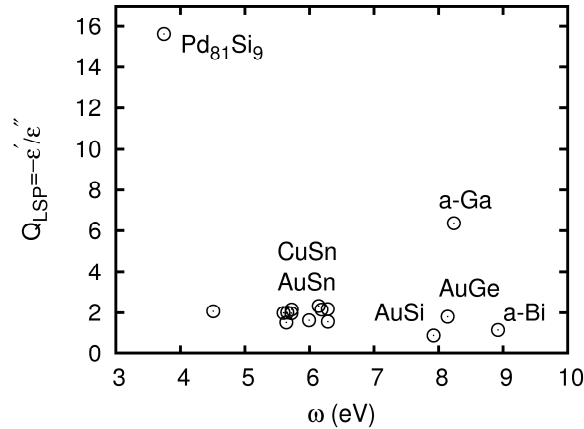
Figure 10. Maximum Q_{LSP} for a variety of metallic glasses using plasma frequencies and drude damping parameters collated by Mitzutani [140]. The materials have varying stoichiometries defined by A_xB_{100-x}. The AuSi [138] and AuGe have $x=75$ and $x=70$.

With the exception of amorphous PdSi and amorphous Ga, a majority of the glasses reviewed by Mitzutani [140] in figure 10 have poor optical properties.

The optical constants of the amorphous alloys of Ag_xSn_{1-x} and Au_xSn_{1-x} were measured at a single wavelength by Loistl and Baumann [141]. They approximate the intraband damping parameter and show that it is greatest at $x=0.5$ for AuSn and $x=0.66$ for AgSn, reaching values of 2.1 eV in both cases, indicating some sort of additional order at these stoichiometries where chemical bonding begins to occur. Similar effects occur in liquid CsAu, MbBi and LiBi (see [142]).

Amorphous NiP alloys were studied by McKnight *et al* [143]. They show that in the amorphous phase interband transitions are shifted to higher energies with increasing phosphorous content. Unfortunately, although the scattering rate reduces with increasing P, the plasma frequency also decreases. The relationship between the square of the plasma frequency and the scattering rate is linear for P concentrations below about 20 % indicating additional scattering mechanisms begin to appear at these concentrations. In CoP [144] any alloying with phosphorous causes the low energy transition in Co to become unresolvable.

Amorphous Ti and Mo disilicides have inferior plasmonic properties compared to the crystalline compounds studied in section 5 [105]. Amorphous Fe and Cr have a smaller interband component than the crystalline versions, but Kudryavtsev *et al* [105] report no data for the real part of the permittivity.

Summarizing, amorphous and liquid materials exhibit smeared interbands which reduces their impact. However, since most metals require higher temperature to exist as a liquid, electron-electron scattering is typically increased. For most amorphous and liquid materials we surveyed plasmonic performance is worse, however liquid phase Na and Ga exhibit increased performance over their solid state counterparts.

8. Conclusions

We have discussed the optical performance of some different types of materials - including the elemental metals, alloys, intermetallics, silicides – as well as high-pressure and amorphous phases. The silicides and many of the alloys studied here have partially occupied *d*-bands that adversely affect their plasmonic performance. However, dopants may be introduced to disrupt the low energy transitions, giving an overall increase in plasmonic quality. The silicides as well as most liquid and amorphous

materials and doped materials have very large Drude phenomenological scattering rates. We showed that the plasma frequency and band edge of some materials could be shifted substantially with the addition of pressure, however, plasmonic devices working under 40 GPa of pressure is a scientific curiosity at best, and practical applications are difficult to envision. We note the very interesting optical properties of liquid sodium and gallium, and would be very interested in the optical properties of the NaK eutectic, which has a melting point of -30°C.

We conclude that intermetallic compounds are most likely to offer an alternative to silver and gold for plasmonic applications. Materials with simple crystal structures and low lying d-states, are most likely to perform well.

Appendix A

Table A.1) References for the optical properties of the elements presented in Figure 1. In the case where multiple tabulations are available (in particular for Cu, Ag and Au), we chose the optical constants that gave the highest Q_{LSP}. The data is partially sourced from collations by Weaver [73] and Palik [45, 145]. Unpublished data by Weaver and coworkers (V, Hf, Re, Os) made available in [73], is cited as such. Data for Zr is not cited correctly by Weaver and Frederikse [73].

Elements 3-28		Elements 29-49		Elements 50-83	
Li	[146]	Cu	[33]	Sn	[147]
Be	[148]	Zn	[149]	Cs	[150]
Na	[151, 152]	Ga	[135]	Ba	[153]
Mg	[33]	Rb	[150]	Hf	[73]
Al	[127]	Sr	[153]	Ta	[154]
K	[152, 155]	Y	[156]	W	[56]
Ca	[149]	Zr	[73]	Re	[73]
Sc	[157]	Nb	[158]	Os*	[73]
Ti	[159]	Mo	[154]	Ir	[160]
V	[73]	Ru	[73]	Pt	[161]
Cr	[162]	Rh	[160]	Au	[73]
Mn	[159, 163]	Pd	[164]	Hg	[165]
Fe	[166]	Ag	[33]	Tl	[167]
Co	[166]	Cd	[149]	Pb	[168]
Ni	[169]	In	[40]	Bi	[170]

References

[1]   Schurig, D., J. J. Mock, B. J. Justice, S. A. Cummer, J. B. Pendry, A. F. Starr, and D. R. Smith 2006 *Science* **314** 977

2   Kneipp, K., Y. Wang, H. Kneipp, L. T. Perelman, I. Itzkan, R. R. Dasari, and M. S. Feld 1997 *Phys. Rev. Lett.* **78** 1667

3   Pissuwan, D., S. M. Valenzuela, C. M. Miller, and M. B. Cortie 2007 *Nano Lett.* **7** 3808

4   Engheta, N. 2007 *Science* **317** 1698

5   MacDonald, K. F., Z. L. Samson, M. I. Stockman, and N. I. Zheludev 2009 *Nat. Photon.* **3** 55

6   Krasavin, A. V. and N. I. Zheludev 2004 *Appl. Phys. Lett.* **84** 1416

7   Arnold, M. D. and M. G. Blaber 2009 *Opt. Express* **17** 3835

8   Ramakrishna, S. A. and J. B. Pendry 2003 *Phys. Rev. B* **67** 201101

9   Noginov, M. A., G. Zhu, M. Bahoura, J. Adegoke, C. E. Small, B. A. Ritzo, V. P. Drachev, and V. M. Shalaev 2006 *Opt. Lett.* **31** 3022

10   Maier, S. A. 2006 *Opt. Commun.* **258** 295

11   Bratkovsky, A., E. Ponizovskaya, S.-Y. Wang, P. Holmstrom, L. Thylen, Y. Fu, and H. Agren 2008 *Appl. Phys. Lett.* **93** 193106

12   Grandidier, J., G. C. des Francs, S. Massenot, A. Bouhelier, L. Markey, J.-C. Weeber, C. Finot, and A. Dereux 2009 *Nano Lett.* **9** 2935

13   Kuttge, M., E. J. R. Vesseur, J. Verhoeven, H. J. Lezec, H. A. Atwater, and A. Polman 2008 *Appl. Phys. Lett.* **93** 113110

14   Ruppin, R. and H. Yatom 1976 *Phys.Status Solidi B* **74** 647

15   Moroz, A. 2008 *J. Phys. Chem. C* **112** 10641

16   Martin, D. S., N. P. Blanchard, P. Weightman, D. S. Roseburgh, R. J. Cole, J. K. Hansen, J. Bremer, and O. Hunderi 2007 *Phys. Rev. B* **76** 115403

17   Lee, M. J. G., M. Gensch, A. I. Shkrebtii, T. Herrmann, W. Richter, N. Esser, and P. Hofmann 2005 *Phys. Rev. B* **72** 085408

18   Stranik, O., R. Nooney, C. McDonagh, and B. MacCraith 2007 *Plasmonics* **2** 15

19   Link, S., Z. L. Wang, and M. A. El-Sayed 1999 *J. Phys. Chem. B* **103** 3529

20   Mallin, M. P. and C. J. Murphy 2002 *Nano Lett.* **2** 1235

21   Chiu, H.-K., I. C. Chiang, and D.-H. Chen 2009 *J. Nanopart. Res.* **11** 1137

22   Hambrock, J., M. K. Schroter, A. Birkner, C. Woll, and R. A. Fischer 2003 *Chem. Mater.* **15** 4217

23   Chou, N. H. and R. E. Schaak 2007 *J. Am. Chem. Soc.* **129** 7339

24   Smith, D. R., W. J. Padilla, D. C. Vier, S. C. Nemat-Nasser, and S. Schultz 2000 *Phys. Rev. Lett.* **84** 4184

25   Ferrando, R., J. Jellinek, and R. L. Johnston 2008 *Chem. Rev.* **108** 845

26   Andrews, M. P. and S. C. O'Brien 2002 *J. Phys. Chem-US* **96** 8233

27   Cortie, M. B., A. Maaroof, G. B. Smith, and P. Ngoepe 2006 *Curr. Appl. Phys.* **6** 440

28   Basit, L., et al. 2009 *J. Phys. D: Appl. Phys.* **42** 084018

29   Cable, R. E. and R. E. Schaak 2007 *Chem. Mater.* **19** 4098

30   West, P., S. Ishii, G. Naik, N. Emani, V. M. Shalaev, and A. Boltasseva 2009 **(arXiv:0911.2737v3)**

31   Maksimov, E. G., I. I. Mazin, S. N. Rashkeev, and Y. A. Uspenski 1988 *J. Phys. F: Met. Phys.* **18** 833

32   Blaber, M. G., M. D. Arnold, and M. J. Ford 2010 **(arXiv:0908.3707v1)**

33   Hagemann, H. J., W. Gudat, and C. Kunz 1975 *J. Opt. Soc. Am.* **65** 742

34   Johnson, P. B. and R. W. Christy 1972 *Phys. Rev. B* **6** 4370

35   Drachev, V. P., U. K. Chettiar, A. V. Kildishev, H.-K. Yuan, W. Cai, and V. M. Shalaev 2008 *Opt. Express* **16** 1186

36   Blaber, M. G., M. D. Arnold, and M. J. Ford 2009 *J. Phys. Chem. C* **113** 3041

37   Blaber, M. G., M. D. Arnold, N. Harris, M. J. Ford, and M. B. Cortie 2007 *Physica B* **394** 184

38   Blaber, M. G., N. Harris, M. J. Ford, and M. B. Cortie, in *International Conference on Nanoscience and Nanotechnology, 2006. ICONN '06.* (IEEE, Brisbane, Australia, 2006), p. 561.

39   McMahon, J. M., S. K. Gray, and G. C. Schatz 2009 **(arXiv:0908.2000v1)**

40   Koyama, R. Y., N. V. Smith, and W. E. Spicer 1973 *Phys. Rev. B* **8** 2426

41   Gasche, T., M. S. S. Brooks, and B. Johansson 1996 *Phys. Rev. B* **54** 2446

42   Fäldt, Å. and P. O. Nilsson 1980 *Phys. Rev. B* **22** 1740

43 Faldt, A. and P. O. Nilsson 1980 *J. Phys. F: Met. Phys.* **10** 2573

44 Quemerais, A., B. Loisel, G. Jezequel, J. Thomas, and J. C. Lemonnier 1981 *J. Phys. F: Met. Phys.* **11** 293

45 Palik, E. D., *Handbook of Optical Constants of Solids III* (Academic Press, 1998).

46 Sharma, A. K. and G. J. Mohr 2008 *J. Phys. D Appl. Phys.* **41** 055106

47 Sharma, A. K., H. S. Pattanaik, and G. J. Mohr 2009 *J. Phys. D Appl. Phys.* **42** 045104

48 Roy, R. K., S. K. Mandal, and A. K. Pal 2003 *Euro. Phys. J. B.* **33** 109

49 Rivory, J. 1977 *Phys. Rev. B* **15** 3119

50 Soven, P. 1967 *Phys. Rev.* **156** 809

51 Inagaki, T., E. T. Arakawa, R. D. Birkhoff, and M. W. Williams 1976 *Phys. Rev. B* **13** 5610

52 Inagaki, T., L. C. Emerson, E. T. Arakawa, and M. W. Williams 1976 *Phys. Rev. B* **13** 2305

53 Petrakian, J. P., A. R. Cathers, J. E. Parks, R. A. MacRae, T. A. Callcott, and E. T. Arakawa 1980 *Phys. Rev. B* **21** 3043

54 Song, J., H. Li, J. Li, S. Wang, and S. Zhou 2002 *Appl. Opt.* **41** 5413

55 Kreibig, U. and M. Vollmer, *Optical properties of metal clusters* (Springer-Verlag, Berlin Heidelberg, 1995).

56 Weaver, J. H., C. G. Olson, and D. W. Lynch 1975 **12** 1293

57 Beaglehole, D. and E. Erlbach 1972 *Phys. Rev. B* **6** 1209

58 DeReggi, A. S. and R. S. Rea 1973 *Phys. Rev. Lett.* **30** 549

59 Nastasi-Andrews, R. J. and R. E. Hummel 1977 *Phys. Rev. B* **16** 4314

60 Korn, D., H. Pfeifle, and G. Zibold 1979 *J Phys. F: Met. Phys.* **9** 1709

61 Myers, H. P., L. Wallden, and A. Karlsson 1968 *Philos. Mag.* **18** 725

62 Flaten, C. J. and E. A. Stern 1975 *Phys. Rev. B* **11** 638

63 Modesti, S., R. Rosei, and E. Colavita 1977 *Il Nuovo Cimento B (1971-1996)* **39** 442

64 Kim, K. J., L.-Y. Chen, and D. W. Lynch 1988 *Phys. Rev. B* **38** 13107

65 Bassett, M. and D. Beaglehole 1976 *J Phys. F: Met. Phys.* **6** 1211

66 Thomas, L. K. and S. Thurm 1976 *J Phys. F: Met. Phys.* **6** 279

67 Ratajack, M. T., K. Kishio, J. O. Brittain, and C. R. Kannewurf 1980 *Phys. Rev. B* **21** 2144

68 Kezuka, H. 1976 *Jpn. J Appl. Phys.* **15** 895

69 Kezuka, H. 1976 *Thin Solid Films* **36** 161

70 Ashcroft and Mermin, *Solid State Physics* (Saunders College Publishing, 1976).

71 Blaber, M. G., M. D. Arnold, and M. J. Ford 2009 *J. Phys-Cond. Mat.* **21** 144211

72 Palik, E. D., *Handbook of Optical Constants of Solids* (Academic Press, 1985).

73 Weaver, J. H. and H. P. R. Frederikse, *Optical properties of selected elements 82 ed.* (CRC Press, Boca Raton, FL, 2001).

74 Scott, W. and L. Muldawer 1974 *Phys. Rev. B* **9** 1115

75 Skriver, H. L. and H. P. Lengkeek 1979 *Phys. Rev. B* **19** 900

76 Lange, R. J., S. J. Lee, D. W. Lynch, P. C. Canfield, B. N. Harmon, and S. Zollner 1998 *Phys. Rev. B* **58** 351

77 Hsu, L.-S. 1994 *Mod. Phys. Lett. B* **8** 1297

78 Heycock, C. T. and F. H. Neville 1900 *Philos. T. R. Soc. Lond.* **194** 201

79 Mitterer, C., H. Lenhart, P. H. Mayrhofer, and M. Kathrein 2004 *Intermetallics* **12** 579

80 Vishnubhatla, S. S. and J. P. Jan 1967 *Philos. Mag.* **16** 45

81 Kim, K. J., B. N. Harmon, L.-Y. Chen, and D. W. Lynch 1990 *Phys. Rev. B* **42** 8813

82 Irani, G. B., T. Huen, and F. Wooten 1971 *Phys. Rev. B* **3** 2385

83 Jan, J. P. and S. S. Vishnubhatla 1967 *Can. J. Phys.* **45** 2505

84 Tarafder, K., A. Chakrabarti, K. K. Saha, and A. Mookerjee 2006 *Phys. Rev. B* **74** 144204

85 Schlemper, K. and L. K. Thomas 1994 *Phys. Rev. B* **50** 17802

86 van der Heide, P. A. M., J. J. M. Buiting, L. M. ten Dam, L. W. M. Schreurs, R. A. de Groot, and A. R. de Vroomen 1985 *J. Phys. F: Met. Phys.* **15** 1195

87 Hsu, L. S. and Y. K. Wang 2004 *J. Alloy Compd.* **377** 29

88 Kim, K. J., B. N. Harmon, and D. W. Lynch 1991 *Phys. Rev. B* **43** 1948

89 Rhee, J. Y. 2006 *Curr. Appl. Phys.* **6** 852

90 Rhee, J. Y. 2004 *J. Appl. Phys.* **96** 7018

91   Antonov, V. N., O. V. Krasovska, E. E. Krasovskii, Y. V. Kudryavtsev, V. V. Nemoshkalenko, B. Y. Yavorsky, Y. P. Lee, and K. W. Kim 1997 *J. Phys-Cond. Mat.* **9** 11227

92   Lee, S. J., J. M. Park, P. C. Canfield, and D. W. Lynch 2003 *Phys. Rev. B* **67** 075104

93   Kim, K. J. 1992 *J. Phys-Cond. Mat.* **4** 8039

94   Nautiyal, T., S. Auluck, P. Blaha, and C. Ambrosch-Draxl 2000 *Phys. Rev. B* **62** 15547

95   Lee, S. J., J. M. Park, T. A. Wiener, L. L. Miller, and D. W. Lynch 2001 *Phys. Rev. B* **64** 125112

96   Kubo, Y., S. Ishida, and J. Ishida 1981 *J. Phys. F: Met. Phys.* **11** 2443

97   Kudryavtsev, Y. V., V. A. Oksenenko, N. N. Lee, Y. P. Lee, J. Y. Rhee, and J. Dubowik 2005 *J. Appl. Phys.* **97** 113903

98   Kudryavtsev, Y. V., Y. P. Lee, and J. Y. Rhee 2002 *Phys. Rev. B* **66** 115114

99   Kudryavtsev, Y. V., Y. P. Lee, and J. Y. Rhee 2004 *Phys. Rev. B* **69** 195104

100   Shreder, E., S. V. Streltsov, A. Svyazhin, A. Makhnev, V. V. Marchenkov, A. Lukoyanov, and H. W. Weber 2008 *J. Phys-Cond. Mat.* **20** 045212

101   Shreder, E. I., M. M. Kirillova, and V. P. Dyakina 2003 *Phys Met. Metallogr+* **96** 467

102   Zwilling, M., P. C. Schmidt, and A. Weiss 1978 *Appl. Phys. A-Mater.* **16** 255

103   Zhang, S.-L. and M. Ostling 2003 *Crit. Rev. Solid. State.* **28** 1

104   Soref, R., R. E. Peale, and W. Buchwald 2008 *Opt. Express* **16** 6507

105   Kudryavtsev, Y. V., M. V. Belous, Y. N. Makogon, S. I. Sidorenko, and T. T. Silakova 1997 *Microelectron. Eng.* **37-38** 559

106   Nava, F., et al. 1993 *Mater. Sci. Rep.* **9** 141

107   Kim, K. J., K. Ji Hoon, B. Jae Ho, L. Myoung Hee, and D. W. Lynch 1997 *J. Appl. Phys.* **82** 4043

108   Imai, Y. and A. Watanabe 2009 *J. Alloy. Compd.* **478** 754

109   Affronte, M., O. Laborde, G. L. Olcese, and A. Palenzona 1998 *J. Alloy. Compd.* **274** 68

110   Migas, D. B., V. L. Shaposhnikov, and V. E. Borisenko 2007 *Phys. Status Solidi B* **244** 2611

111   Henle, W. A., M. G. Ramsey, F. P. Netzer, R. Cimino, W. Braun, and B. GmbH 1989 *Solid State Commun.* **71** 657

112   Hofmann, R., W. A. Henle, F. P. Netzer, and M. Neuber 1992 *Phys. Rev. B* **46** 3857

113   Kudryavtsev, Y. V., V. A. Oksenenko, Y. P. Lee, J. Y. Rhee, and Y. D. Kim 2007 *J. Appl. Phys.* **102** 103503

114   Wu, Z. C., E. T. Arakawa, J. R. Jimenez, and L. J. Schowalter 1992 *J. Appl. Phys.* **71** 5601

115   Hanfland, M., K. Syassen, N. E. Christensen, and D. L. Novikov 2000 *Nature* **408** 174

116   Christensen, N. E. and D. L. Novikov 2006 *Phys. Rev. B* **73** 224508

117   Profeta, G., et al. 2006 *Phys. Rev. Lett.* **96** 047003

118   Alonso, R. E., S. Sharma, C. Ambrosch-Draxl, C. O. Rodriguez, and N. E. Christensen 2006 *Phys. Rev. B* **73**

119   Rodriguez-Prieto, A., V. M. Silkin, A. Bergara, and P. M. Echenique 2008 *New J. Phys.* **10** 053035

120   Alouani, M., N. E. Christensen, and K. Syassen 1989 *Phys. Rev. B* **39** 8096

121   Gao, G., Y. Xie, T. Cui, Y. Ma, L. Zhang, and G. Zou 2008 *Solid State Commun.* **146** 181

122   Hatton, J. 1955 *Phys. Rev.* **100** 681

123   Sundqvist, B., J. Neve, and Ö. Rapp 1985 *Phys. Rev. B* **32** 2200

124   Li, Q., Y. Li, T. Cui, Y. Wang, L. J. Zhang, Y. Xie, Y. L. Niu, Y. M. Ma, and G. T. Zou 2007 *J. Phys-Condens. Mat.* **19** 425224

125   Helman, J. S. and W. Baltensperger 1977 *Phys. Rev. B* **15** 4109

126   Krishnan, S. and P. C. Nordine 1993 *Phys. Rev. B* **47** 11780

127   Shiles, E., T. Sasaki, M. Inokuti, and D. Y. Smith 1980 *Phys. Rev. B* **22** 1612

128   Huttner, B. 1994 *J. Phys-Condens. Mat.* **6** 2459

129   Krasavin, A. V., K. F. MacDonald, A. S. Schwanecke, and N. I. Zheludev 2006 *Appl. Phys. Lett.* **89** 031118

130   MacDonald, K. F., A. V. Krasavin, and N. I. Zheludev 2007 *Opt. Commun.* **278** 207

131   Miller, J. C. 1969 *Philos. Mag.* **20** 1115

132   Hodgson, J. N. 1961 *Philos. Mag.* **6** 509

133   Inagaki, T., E. T. Arakawa, A. R. Cahters, and K. A. Glastad 1982 *Phys. Rev. B* **25** 6130

[134] Hodgson, J. N. 1967 *Adv. Phys.* **16** 675

[135] Jezequel, G., J. C. Lemonnier, and J. Thomas 1977 *J. Phys. F: Met. Phys.* **7** 1613

[136] Schulz, L. G. 1957 *J. Opt. Soc. Am.* **47** 64

[137] Fuchs, M. S. K. 2000 *J. Phys-Condens. Mat.* **12** 4341

[138] Hauser, E., R. J. Zirke, J. Tauc, J. J. Hauser, and S. R. Nagel 1979 *Phys. Rev. B* **19** 6331

[139] Hauser, E., R. J. Zirke, J. Tauc, J. J. Hauser, and S. R. Nagel 1978 *Phys. Rev. Lett.* **40** 1733

[140] Mizutani, U. 1983 *Prog. Mater. Sci.* **28** 97

[141] Loistl, M. and F. Baumann 1992 *Zeitschrift für Physik B Condensed Matter* **89** 71

[142] Schmutzler, R. W., H. Hoshino, R. Fischer, and F. Hensel 1976 *Ber. Bunsen-Ges. Phys. Chem. Chem. Phys.* **80** 107

[143] McKnight, S. W. and A. K. Ibrahim 1984 *Phys. Rev. B* **29** 6570

[144] Rivory, J. and B. Bouchet 1979 *J. Phys. F: Met. Phys.* **9** 327

[145] Palik, E. D., *Handbook of Optical Constants of Solids II* (Academic Press, 1991).

[146] Rasigni, M. and G. Rasigni 1977 *J. Opt. Soc. Am.* **67** 54

[147] MacRae, R. A., E. T. Arakawa, and M. W. Williams 1967 *Phys. Rev.* **162** 615

[148] Weaver, J. H., D. W. Lynch, and R. Rosei 1973 *Phys. Rev. B* **7** 3537

[149] Lenham, A. P. and D. M. Treherne 1964 *P. Phys. Soc.* **83** 1059

[150] Smith, N. V. 1970 *Phys. Rev. B* **2** 2840

[151] Sutherland, J. C., E. T. Araiawa, and R. N. Hamm 1967 *J. Opt. Soc. Am.* **57** 645

[152] Smith, N. V. 1969 *Phys. Rev.* **183** 634

[153] Endriz, J. G. and W. E. Spicer 1970 *Phys. Rev. B* **2** 1466

[154] Weaver, J. H., D. W. Lynch, and C. G. Olson 1974 *Phys. Rev. B* **10** 501

[155] Whang, U. S., E. T. Arakawa, and T. A. Callcott 1972 *Phys. Rev. B* **6** 2109

[156] Weaver, J. H. and C. G. Olson 1977 *Phys. Rev. B* **15** 590

[157] Sigrist, M., G. Chassaing, J. C. François, F. Antonangeli, N. Zema, and M. Piacentini 1987 *Phys. Rev. B* **35** 3760

[158] Weaver, J. H. and C. G. Olson 1977 *Phys. Rev. B* **16** 731

[159] Johnson, P. B. and R. W. Christy 1974 *Phys. Rev. B* **9** 5056

[160] Weaver, J. H., C. G. Olson, and D. W. Lynch 1977 *Phys. Rev. B* **15** 4115

[161] Weaver, J. H. 1975 *Phys. Rev. B* **11** 1416

[162] Bos, L. W. and D. W. Lynch 1970 *Phys. Rev. B* **2** 4567

[163] Fouad, S. S. and A. H. Ammar 1995 *Physica B* **205** 285

[164] Weaver, J. H. and R. L. Benbow 1975 *Phys. Rev. B* **12** 3509

[165] Inagaki, T., E. T. Arakawa, and M. W. Williams 1981 *Phys. Rev. B* **23** 5246

[166] Weaver, J. H., E. Colavita, D. W. Lynch, and R. Rosei 1979 *Phys. Rev. B* **19** 3850

[167] Jézéquel, G., J. Thomas, and I. Pollini 1988 *Phys. Rev. B* **37** 8639

[168] Lemonnier, J. C., M. Priol, and S. Robin 1973 *Phys. Rev. B* **8** 5452

[169] Lynch, D. W., R. Rosei, and J. H. Weaver 1971 *Solid State Commun.* **9** 2195

[170] de Sande, J. C. G., T. Missana, and C. N. Afonso 1996 *J. Appl. Phys.* **80** 7023